Calculation of Unary Phase Diagrams for Pure Nickel

Anirudh Bali

10/29/2025

1. Introduction

Calculation of phase diagrams is central to the practice of materials thermodynamics. This study calculates the unary phase diagrams for pure nickel (Ni). Specifically, field-field, field-density, and density-density type phase diagrams are calculated solely from specific heat capacity data and the thermophysical properties of Ni using thermodynamic principles.

This study is Part III of an ongoing materials thermodynamics project being completed for the Fall 2025 session of MTEN 6005 taught by Dr. Eric Payton. The overall objective of this project is to calculate a binary phase diagram not published in the SGTE collection of publicly available binary datasets [1]. Each part of the project builds on the results of previous parts to work towards this objective. In Part I, enthalpy and entropy functions for Ni were calculated using specific heat capacity data [2]. In Part II, the triple point for Ni was calculated using Gibbs free energy functions and the method of Lagrange multiples [3]. This study starts with improving the triple point calculations presented in Part II to define more accurate Gibbs free energy functions for the solid, liquid, and gas phases of Ni. These functions are then used to calculate the unary phase diagrams.

Portions of the methods (Section 2) and results (Section 3) shared in Part III is material originally presented in Part I and Part II of the project. They have been included in this report for completeness and to establish the theoretical background required to calculate unary phase diagrams. However, Part III's discussion (Section 4) focuses on the results specific to Part III. For a full discussion of Part I and Part II results, refer to their respective reports.

2. Methods

As mentioned, the objective of Part III is to calculate the unary phase diagrams of a pure element (Ni) using specific heat capacity data, thermophysical properties, and thermodynamic principles. The following section outlines the thermodynamic principles and numerical techniques utilized to calculate the phase diagrams of interest.

NIST-JANAF was the source used for temperature dependent specific heat capacity data from 0 K to 6000 K of Ni [4]. Table 1 summarizes select material properties reported by NIST-JANAF that will be utilized to define functions for specific heat capacity, enthalpy, and entropy.

Table 1. NIST-JANAF data for Ni [4]

Standard State Pressure ($P°$)	0.1 MPa
Enthalpy Reference Temperature (T_r)	298.15 K

Table 1 continued. NIST-JANAF data for Ni [4]

C_p Lambda Maximum Transition Temp. (T_λ)	631.000 K
Melting Temperature (T_m)	1728.000 K
Vaporization Temperature (T_v)	3156.584 K
Fugacity	1 bar

Several additional thermophysical properties were needed to calculate the phase diagrams of interest. Table 2 summarizes the additional properties required.

Table 2. Physical Constants and Thermophysical Properties of Ni [5, 6, 7]

Ideal Gas Constant (R)	8.341 J mol^{-1} K^{-1}
Atomic Mass (M)	58.6934 g mol^{-1}
Density of Solid Phase at T_r (ρ_s)	8909 kg m^{-3}
Density of Liquid Phase at T_m (ρ_m)	7810 kg m^{-3}
Linear Thermal Expansion Coefficient (α)	13.3×10^{-6} K^{-1}
Isothermal Compressibility (β)	0.00538 GPa^{-1}

2.1 Deriving Standard State Enthalpy and Entropy Functions

Equation 1 and Equation 2 present two forms of the Shomate equation used to curve fit specific heat capacity data and define $C_p(T)$ of Ni from 0 K to 6000 K. Across this temperature range, Ni undergoes three phase transformations, a solid-to-solid, solid-to-liquid, and liquid-to-gas transformation, occurring at their respective temperatures reported in Table 1. The discontinuities in specific heat capacity data at phase transformations necessitate that $C_p(T)$ is defined as a piecewise function.

$$C_p(T) = a + bT + cT^2 + dT^3 \tag{1}$$

$$C_p(T) = a + bT + cT^2 + dT^3 + \frac{e}{T^2} \tag{2}$$

To calculate the polynomial coefficients for each phase, MATLAB's `fittype` and `fit` function were used. The `fittype` function defined the form of the fitted polynomial and the `fit` function calculated the unknown coefficients [8, 9]. Equation 1, a simplified form of the Shomate equation that excludes the fifth polynomial term, was used to define $C_p(T)$ from 0 K to T_λ as `fit` was unable to calculate the coefficients for Equation 2, the full form of the Shomate equation, due to the highly nonlinear nature of heat capacity in this temperature range. Equation 2 was used to

define specific heat capacity for the remaining temperature ranges (second solid phase from T_λ to T_m, liquid phase T_m to T_v, and gas phase from T_v to 6000 K).

$$H(T) = \int C_p \, dT \tag{3}$$

$$S(T) = \int \frac{C_p}{T} \, dT \tag{4}$$

Equation 3 and Equation 4 were used to derive expressions for enthalpy and entropy as a function of temperature, $H(T)$ and $S(T)$ respectively. Equation 5 and Equation 6 are the general forms of $H(T)$ and $S(T)$ derived from integrating Equation 2, the full form of the Shomate equation. Recognize that the coefficients a through e are the coefficients evaluated when curve-fitting $C_p(T)$ from 0 K to 6000 K and vary with phase.

$$H(T) - H(T_0) = aT + \frac{bT^2}{2} + \frac{cT^3}{3} + \frac{dT^4}{4} - \frac{e}{T} + f \tag{5}$$

$$S(T) - S(T_0) = a \ln T + bT + \frac{cT^2}{2} + \frac{dT^3}{3} - \frac{e}{2T^2} + g \tag{6}$$

Due to the piecewise nature of $C_p(T)$, the unknown integration constants, f and g, vary for each phase. To evaluate the value of f and g for each phase, the $C_p(T)$ Shomate polynomials can be integrated using MATLAB's `integral` function, according to Equation 3 and Equation 4, to establish initial values, $H(T_0)$ and $S(T_0)$, for each phase. This operation is not required for $H(T)$ and $S(T)$ from 0 K to T_λ because the standard enthalpy, $H°(T_r)$, and standard entropy, $S°$, from the NIST-JANAF database can be used instead, Table 3.

MATLAB's `integral` function was unable to numerically integrate Equation 4 from 0 K to 100 K; therefore, entropy is only defined from 100 K to 6000 K. This simplification is acceptable for the purposes of subsequent phase diagram calculations as entropy data from 0 K to 100 K is not critical to calculating the unary phase diagrams of Ni.

Table 3. NIST-JANAF data used in enthalpy and entropy calculations [4]

$H°(T_r)$	0. kJ mol^{-1}
$S°(100\ K)$	7.454 J K^{-1} mol^{-1}

2.2 Defining Gibbs Free Energy Functions

The calculation of a unary phase diagram of Ni amounts to identifying the equilibrium phase, i.e. the lowest energy state, for a given set of thermodynamic properties. To do this, the Gibbs free energy of the solid, liquid, and gas phases of Ni must be defined for the entire temperature range being considered, so the phase with the minimum Gibbs free energy can be known. This means that $H(T)$ and $S(T)$ need to be defined for the entire temperature range being considered for each phase, according to Equation 7.

$$G(T) = H(T) - TS(T) \tag{7}$$

Equations 8-13 define $H(T)$ and $S(T)$ from 0 to 6000 K for the solid, liquid, and gas phases of Ni. Each phase has different coefficients which are assumed to be constant from 0 to 6000 K; therefore, Equations 8-13 are simply the enthalpy and entropy functions already calculated for each phase extrapolated across the entire temperature range of interest. For the solid phase, higher order terms of the Shomate equation were excluded due to unrealistic behavior ($H_{solid}(T) < H_{liquid}(T)$ and $\frac{dH_{solid}}{dT} < 0$) as the function was extrapolated from 0 to 6000 K. Assuming a constant specific heat, $C_{p,solid}(T) = a$, for the solid phase led to a more well-behaved $H_{solid}(T)$.

$$H_{solid}(T) = aT + f_{solid} \tag{8}$$

$$H_{liquid}(T) = aT + \frac{bT^2}{2} + \frac{cT^3}{3} + \frac{dT^4}{4} - \frac{e}{T} + f_{liquid} \tag{9}$$

$$H_{gas}(T) = aT + \frac{bT^2}{2} + \frac{cT^3}{3} + \frac{dT^4}{4} - \frac{e}{T} + f_{gas} \tag{10}$$

$$S_{solid}(T) = a\ln T + g_{solid} \tag{11}$$

$$S_{liquid}(T) = a\ln T + bT + \frac{cT^2}{2} + \frac{dT^3}{3} - \frac{e}{2T^2} + g_{liquid} \tag{12}$$

$$S_{gas}(T) = a\ln T + bT + \frac{cT^2}{2} + \frac{dT^3}{3} - \frac{e}{2T^2} + g_{gas} \tag{13}$$

Using $H(T)$ and $S(T)$ functions defined for each phase, the Gibbs free energy as a function of temperature and pressure can be defined for solid, liquid, and gas phases, Equations 14-16. The additional term in Equations 14-16 compared to Equation 7 is a pressure correction term included to account for the pressure dependence of Gibbs free energy, particularly for the gas phase.

$$G_{solid}(T,P) = H°_{solid}(T) - TS°_{solid}(T) + V_m(P - P°) \quad (14)$$

$$G_{liquid}(T,P) = H°_{liquid}(T) - TS°_{liquid}(T) + V_m(P - P°) \quad (15)$$

$$G_{gas}(T,P) = H°_{gas}(T) - TS°_{gas}(T) + RT\ln\left(\frac{P}{P°}\right) \quad (16)$$

Equations 14-17 can be used to calculate the Gibbs free energy of the solid, liquid, and gas phase of nickel as a function of temperature and pressure. Therefore, these equations are used to determine the equilibrium phase of Ni for a given temperature and pressure condition. It is important to recognize that that this formulation of Gibbs free energy treats Ni gas as an ideal gas.

2.3 Calculation of Triple Point

At the triple point, where solid, liquid, and gas phases coexist at equilibrium, Equation 17 must be satisfied.

$$G_{solid}(T,P) = G_{liquid}(T,P) = G_{gas}(T,P) \quad (17)$$

If Equation 17 is not satisfied, it implies there is at least one phase that has a lower energy state than the others, meaning it will be the thermodynamically favored equilibrium of the material, and the three phases will not coexist at equilibrium. To find the specific temperature and pressure where all three phases can coexist, we must solve for the conditions where the Gibbs free energies of all three phases are simultaneously equal. This requires finding the values of T and P that satisfy Equation 17, which can be expressed as two independent constraint equations, Equation 18 and Equation 19.

$$g(T,P) = G_{solid}(T,P) - G_{liquid}(T,P) \ \ and \ \ g(T,P) = 0 \quad (18)$$

$$h(T,P) = G_{solid}(T,P) - G_{gas}(T,P) \ \ and \ \ h(T,P) = 0 \quad (19)$$

Equation 18 and Equation 19 are used to define the Lagrangian function, Equation 20, which sets ups a constrained optimization problem that can be solved to identify the triple point,

$$\mathcal{L}(T,P,\lambda,\mu) = f(T,P) + \lambda g(T,P) + \mu h(T,P) \quad (20)$$

where $f(T,P)$ is the objective function, $g(T,P)$ and $h(T,P)$ are constraint functions, and λ and μ are Lagrange multiples. Recognize, with this setup, an arbitrary objective function can be defined as the two constraint functions are sufficient to define the system of equations needed to solve for the four unknowns $T, P, \lambda,$ and μ (two constraint functions, each with two partial derivatives). Therefore, for simplicity, calculations in MATLAB were carried out using $f(T,P) = 0$. By solving

this system of equations, what is being calculated is the combination of temperature and pressure that satisfy Equation 17.

To solve the system equation for T and P, MATLAB's `fmincon` function was used. This function is specifically designed to find the minimum of constrained nonlinear multivariable functions numerically [10]. In this case, since $f(T,P) = 0$, `fmincon` is not solving for a true minimum, rather it is simply solving for the conditions that satisfy the two constraint equations (which is a root-finding problem).

2.4 Calculation of Unary Phase Diagrams

Field-field, field-density, and density-density phase diagrams for Ni were calculated for Part III of the project. Figure 1 illustrates what each one of these phase diagrams look like schematically for a unary system.

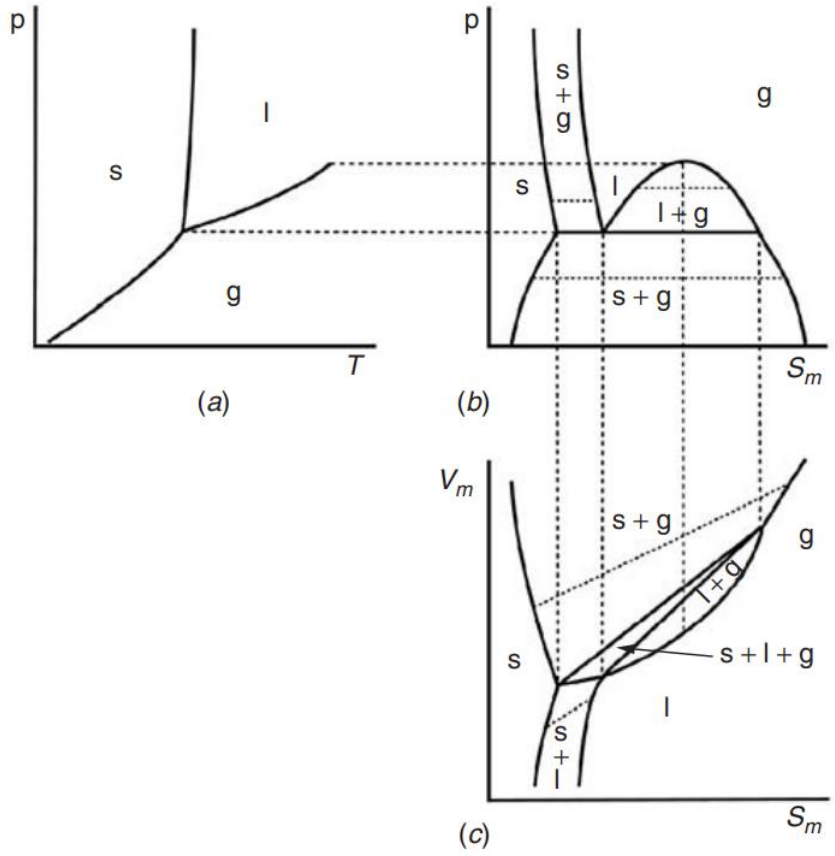

Figure 1. Examples of: (a) field-field, (b) field-density, and (c) density-density phase diagrams. Image originally published in Chapter 4 of Materials Thermodynamics by Chang and Oates [11].

Of particular importance is how the two-phase coexistence curves and triple point on a field-field diagram transform into two-phase, and a three-phase, *areas* as the phase diagram is converted from field-field to field-density to density-density.

The field-field (pressure-temperature) phase diagram was the first to be calculated by: (1) evaluating the Gibbs free energy for solid, liquid, and gas phases using Equation 14-16 for pressure-temperature states across the region of interest, and (2) identifying which phase has the lowest Gibbs free energy for each state. Calculation of the field-field phase diagram in this way makes it straightforward to numerically evaluate the "location" of the two-phase coexistence curves in P-T space and validate the calculated triple point. Identifying the two-phase coexistence curves is significant, as translating these coexistence curves from one domain to another is the key to evaluating field-density and density-density phase diagrams.

For each two-phase coexistence curve (solid-liquid, liquid-gas, and solid-gas), each point along these curves is a fixed thermodynamic state defined fully by temperature and pressure. To convert these phase boundaries to phase boundaries in P-S space, S_m can be calculated using Equations 11-13 for each phase at the boundary being evaluated for all temperatures along the coexistence curve. Therefore, one phase boundary in P-T space results in two phase boundaries in P-S space. Tie-lines connecting the initial and final points of this phase boundary pair establish the two-phase areas in PS-space.

Similarly, to calculate the density-density phase diagram, the molar volume (V_m) of each phase on a coexistence curve needs to be calculated for each pressure-temperature state along the curve. Equation 21-23 can be used to calculate V_m for each phase as a function of temperature and pressure. Plotting the six total phase boundaries (3 two-phase coexistence curves with 2 phases each) and drawing tie lines between phase boundary pairs (i.e. evaluate S_m and V_m for the solid and liquid phase for every point pressure-temperature state on the solid-liquid coexistence curve) illustrates the two-phase areas and three-phase area.

$$V_{m,solid}(T,P) = V_m(T_r)[1 + \alpha(T - T_r) - \beta(P - P°)] \tag{21}$$

$$V_{m,liquid}(T,P) = V_m(T_m)[1 + \alpha(T - T_m) - \beta(P - P°)] \tag{22}$$

$$V_{m,gas}(T,P) = \frac{RT}{P} \tag{23}$$

3. Results

Figure 2 is a plot of specific heat capacity as a function of temperature. NIST-JANAF data points are plotted alongside the curve fit Shomate equations used to estimate the specific heat capacity function used in subsequent calculations for $H(T)$ and $S(T)$. As mentioned, two different

forms of the Shomate equation were used depending on the temperature range the function was being evaluated for. From 0 K to T_λ, corresponding to the red curve in Figure 2, Equation 1 was used due to the highly nonlinear nature of Ni's heat capacity. For $T > T_\lambda$, Equation 2 was used. As highlighted in the graph, the Shomate equations were curve-fit in a piecewise manner to accommodate the discontinuities in specific heat associated with phase transformations. This is represented visually by the different color lines plotted on Figure 2, each corresponding to one temperature range within that piecewise function. Table 4 reports the calculated Shomate coefficients for each phase.

Table 4. Calculated Shomate equation polynomial coefficients (for equations in J mol^{-1})

T [K]	a	b	c	d	e
0 – 631	0.1884	0.1795	– 4.2182 e–04	3.7262 e–07	-
631 – 1728 (S)	33.4004	– 0.0116	1.3094 e–05	– 2.6924 e–09	2.6588 e–04
1728 – 3156.584 (L)	38.9110	0	0	0	0
3156.584 – 6000 (G)	24.8091	– 9.0041 e–04	– 9.9479 e–08	4.5047 e–11	0

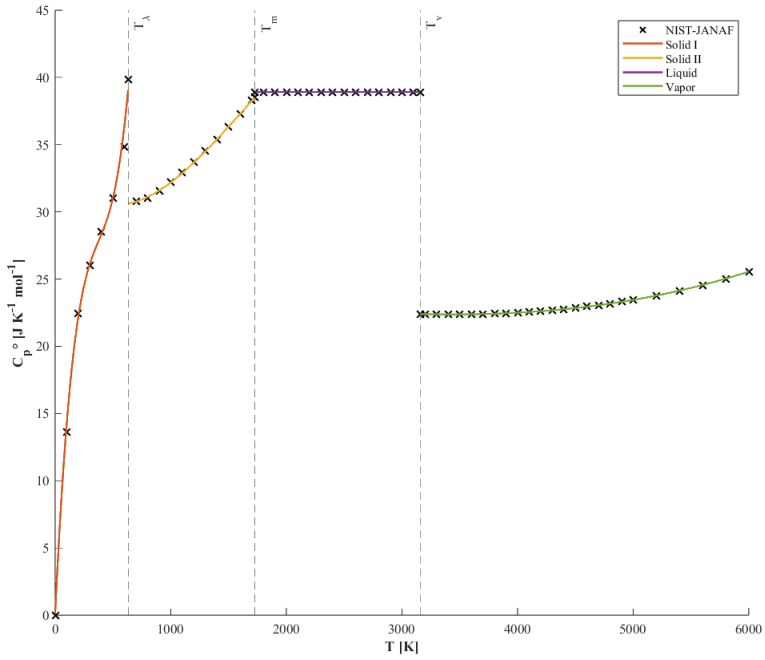

Figure 2. Specific Heat Capacity vs Temperature, Ni

Figure 3 is a plot of enthalpy as a function of temperature. Like specific heat, NIST-JANAF data points are plotted alongside the calculated curves for reference. Note that Equation 3 was used to calculate the enthalpy function for each phase; these curves are not functions calculated through regression of known data points like specific heat capacity. Figure 4 is a plot of entropy as a function of temperature and was calculated similarly to enthalpy using Equation 4. For Figure 1-3, the calculated results show strong agreement with the NIST-JANAF dataset values.

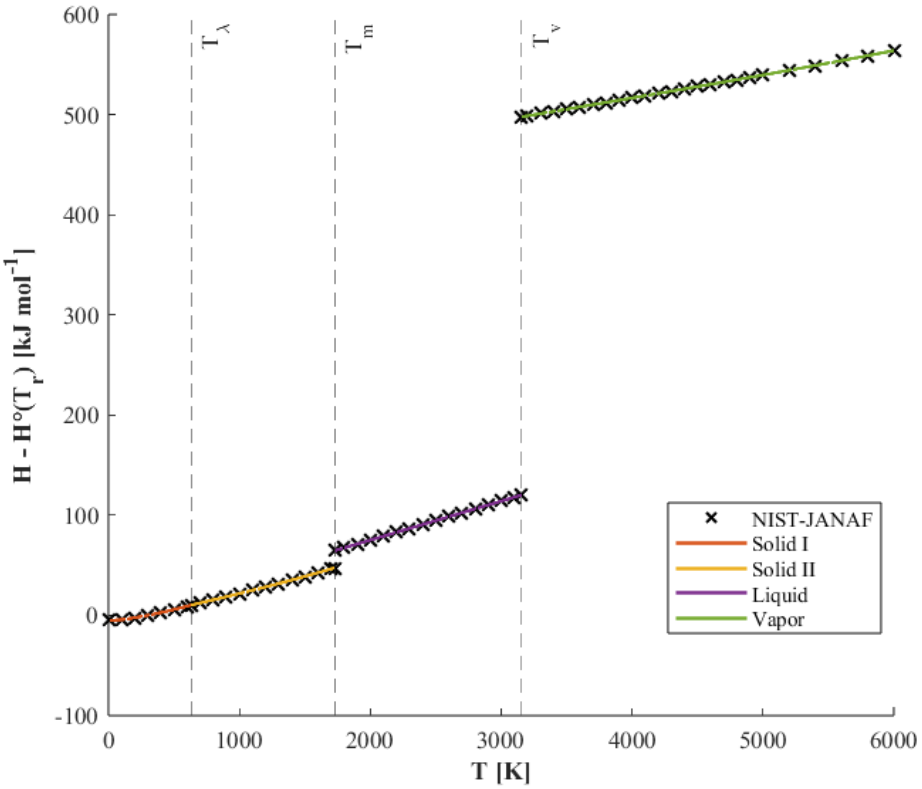

Figure 3. Enthalpy vs Temperature, Ni (above)

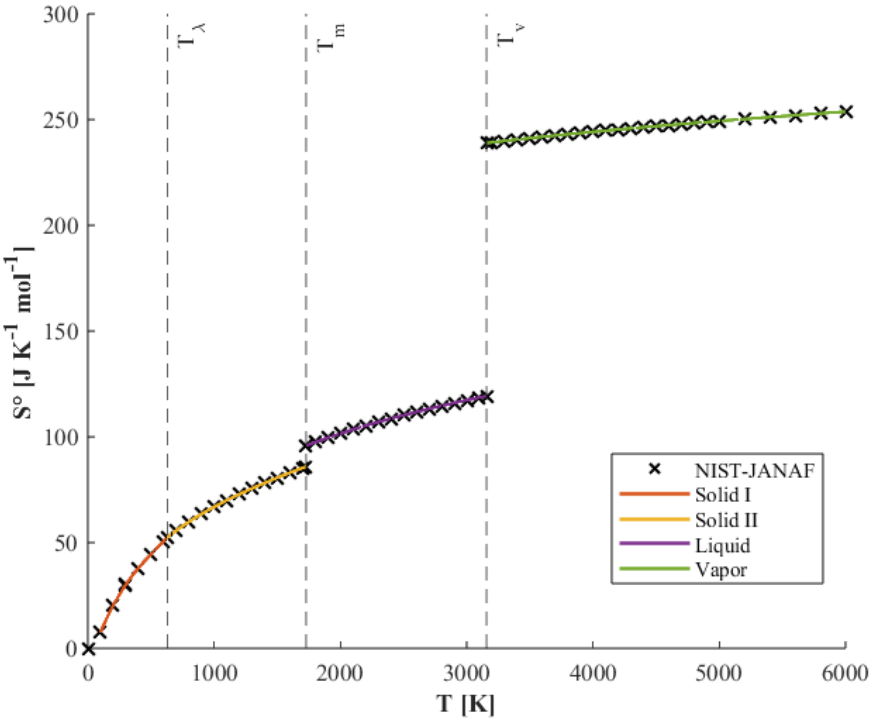

Figure 4. Entropy vs Temperature, Ni

Figure 5 illustrates plots of Equation 8-10 and Equation 11-13 respectively. These equations are plotted alongside NIST-JANAF enthalpy and entropy data for reference. These fits are a significant improvement compared to the `spline` utilized in Part II. Specifically, $H_{solid}(T)$ and $S_{solid}(T)$ are more "well-behaved" as they stay below and liquid curve and monotonically increase with temperature. Table 5 reports the integration constants calculated for Equations 8-13.

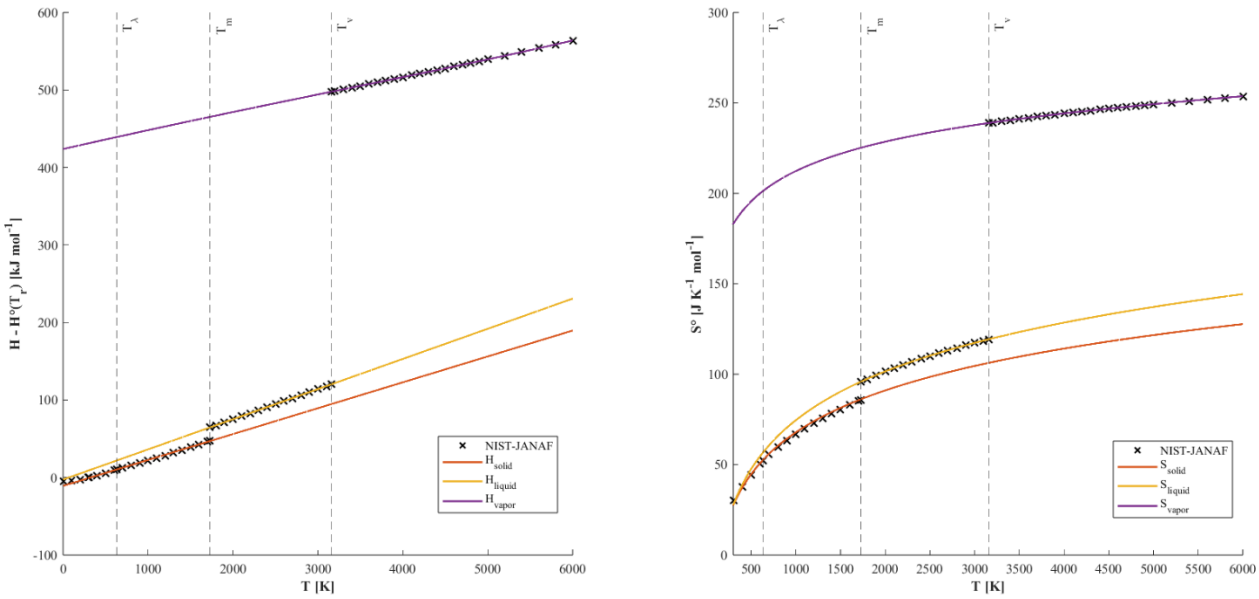

Figure 5. Extrapolated $H_{solid}, H_{liquid}, H_{vapor}$ (left) and extrapolated $S_{solid}, S_{liquid}, S_{vapor}$ (right)

Table 5. Calculated integration constants for Equation 8-13 (in kJ mol^{-1} and J mol^{-1} K^{-1} respectively)

f_{solid}	f_{liquid}	f_{gas}	g_{solid}	g_{liquid}	g_{gas}
– 10.823	– 2.6941	423.78	– 162.8893	– 194.2502	41.8453

Table 6 reports the calculated triple point of Ni by solving the system of equations derived from Equations 18-20 using MATLAB's `fmincon` function. The function met the default stopping criteria and converged in six iterations.

Table 6. Calculated triple point for Ni

T_t	1814.8 K
P_t	1.6685 Pa

Figure 6 illustrates the field-field phase diagram (pressure-temperature) calculated for pure Ni. Each single-phase region is uniquely colored, and the triple point reported in Table 6 is plotted as a red dot. Figure 7 illustrates the calculated field-density phase diagram (pressure-molar entropy).

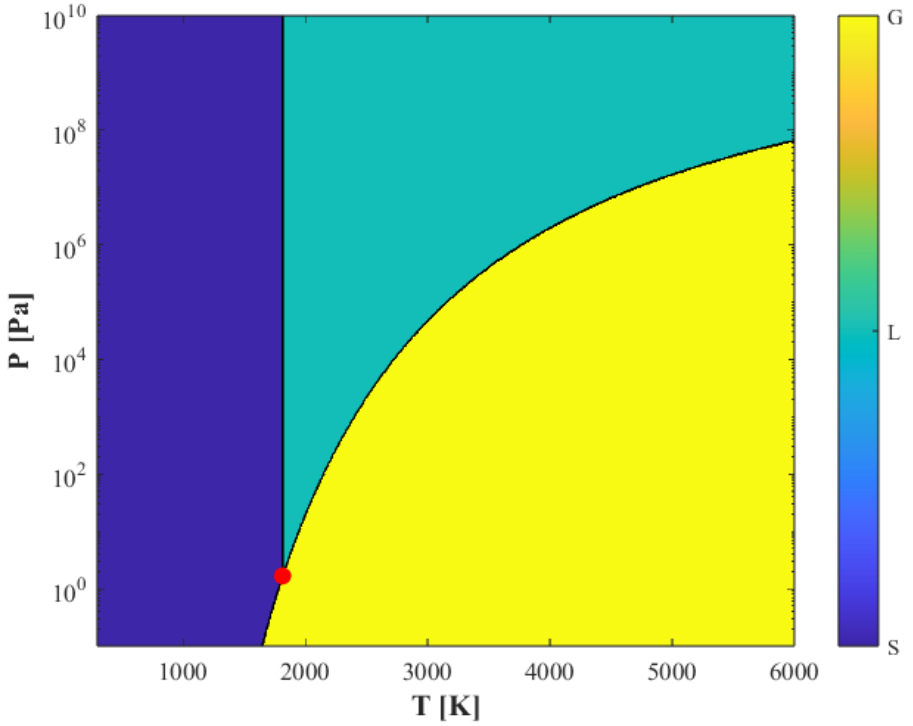

Figure 6. Field-Field Phase Diagram, Ni (above)

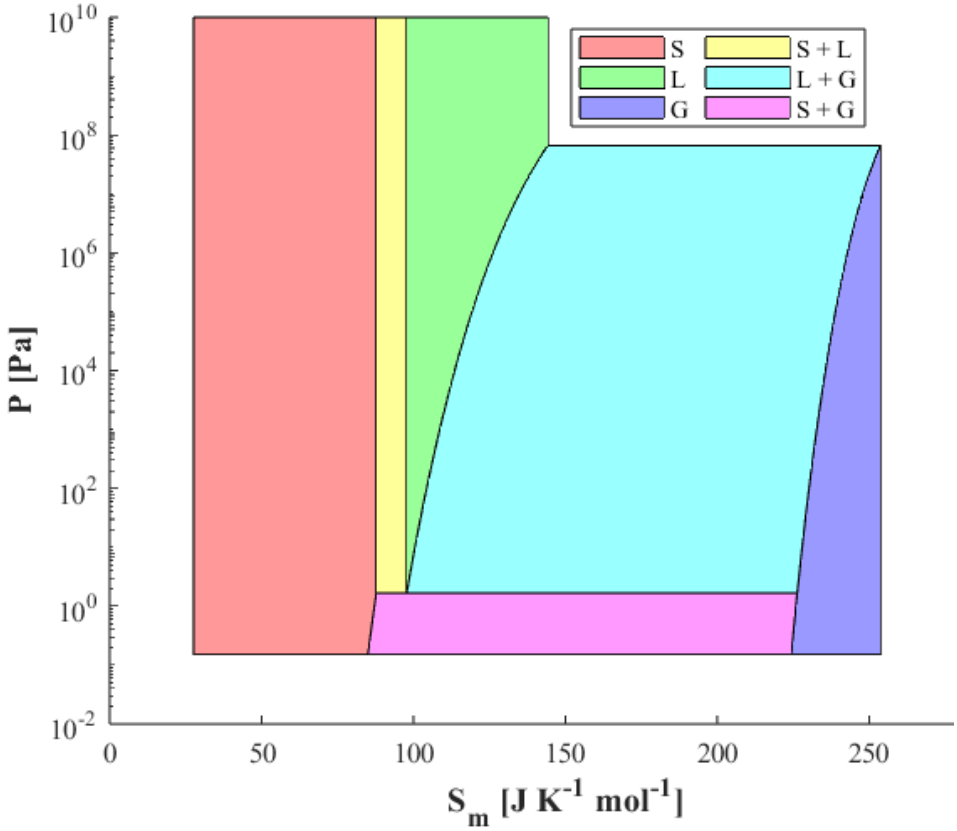

Figure 7. Field-Density Phase Diagram, Ni

Figure 8 and Figure 9 are both illustrations of the calculated density-density phase diagrams (molar volume-molar entropy) of pure Ni. Figure 9 zooms into regions/features of the phase diagram that are too small to see in Figure 8 when the entire search space is being visualized.

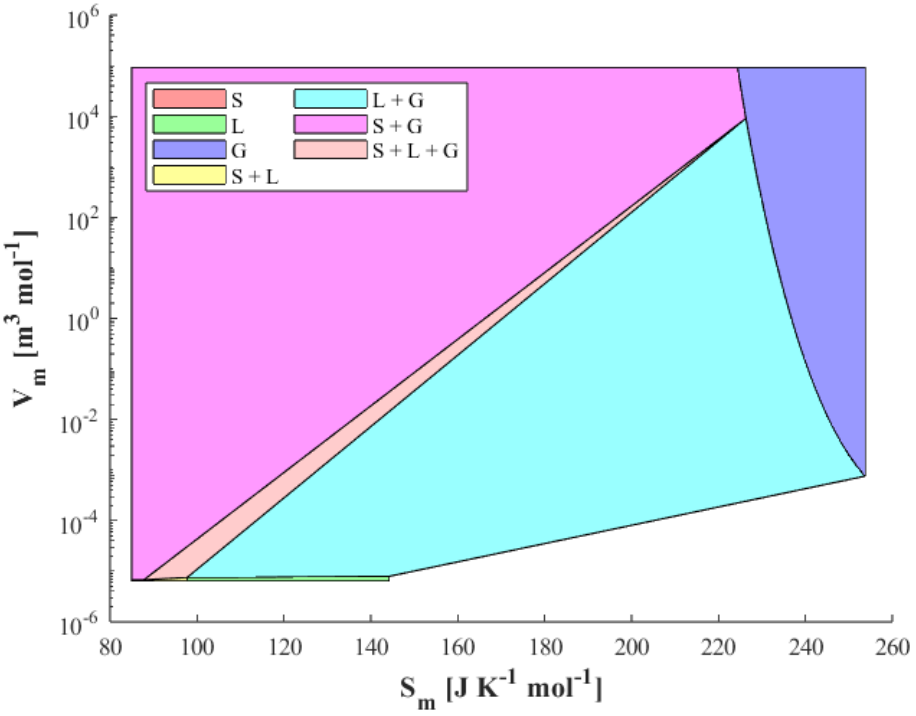

Figure 8. Density-Density Phase Diagram, Ni (above)

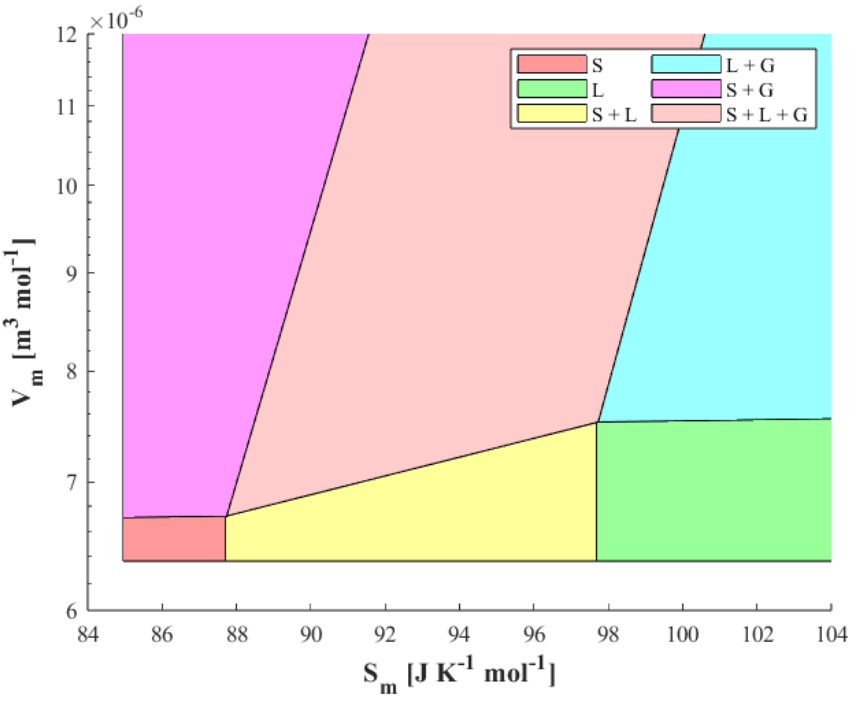

Figure 9. Zoomed-In Density-Density Phase Diagram, Ni

4. Discussion

Part III of the MTEN 6005 project extended the results of Part I and Part II by calculating the unary phase diagram of a pure element. This required improving the extrapolated solid, liquid, and gas enthalpy and entropy functions to ensure well-behaved thermodynamic behavior and applying the thermodynamic principles to identify phase boundaries for a field-field, field-density, and density-density phase diagram.

4.1 Improvements to Single-Phase Enthalpy and Entropy Functions

A critical improvement in Part III compared to Part II involves the reformulation of the extrapolated solid, liquid, and gas enthalpy and entropy to ensure well-behaved thermodynamic behavior across the entire temperature range of interest, 0 K to 6000 K. In Part II, spline interpolation was used to extrapolate these thermodynamic functions beyond their physical temperature range. This method produced physically unrealistic behavior for the solid phase at high temperatures, introducing inaccuracies to subsequent thermodynamic calculations.

The improved formulation presented in Equations 8–13 addresses these inaccuracies by employing temperature-dependent polynomial expressions derived directly from the curve-fit Shomate equation for each phase. Additionally, for the solid phase, the extrapolated functions were simplified to assume constant specific heat capacity, yielding linear enthalpy and logarithmic entropy relationships. This simplification, while reducing mathematical complexity, produces thermodynamically consistent behavior. The solid phase enthalpy remains below that of the liquid phase across all temperatures, and the enthalpy derivative with respect to temperature remains positive, as required by the second law of thermodynamics.

Figure 5 demonstrates the improvement in the approach used in Part III. The functions $H_{solid}(T)$ and $S_{solid}(T)$ exhibit the expected monotonic increases with temperature and maintain physically reasonable relative to the liquid and gas phases. In the earlier spline-based approach, the $H_{solid}(T)$ and $S_{solid}(T)$ exceeded $H_{liquid}(T)$ and $S_{liquid}(T)$ at the same T, which violates fundamental thermodynamic principles. This improved functional form is particularly critical for accurate phase diagram calculations. The Gibbs free energy of each phase, which is used to evaluate phase boundaries, are directly calculated from these enthalpy and entropy functions. Physically unrealistic extrapolations would propagate through the calculations, producing incorrect phase boundary predictions.

4.2 Calculation of Unary Phase Diagrams

Three unary phase diagrams were calculated for Ni – a field-field, field-density, and density-density phase diagram. In this context, *field* refers to an intensive thermodynamic property that can have a spatial dependence within a system (i.e. temperature, pressure, chemical potential) and

density refers to an intensive thermodynamic property that does not vary spatially (i.e. molar volume, molar entropy). Pressure-temperature (P-T), pressure-molar entropy (P-S), and molar volume-molar entropy (V-S) phase diagrams were calculated to evaluate one field-field, one field-density, and one density-density phase diagram respectively.

Figure 6 illustrates the field-field (P-T) phase diagram calculated. The P-T phase diagram shows three single-phase regions corresponding to the pressure-temperature states that will result in a single solid, liquid, or gas phase at equilibrium. Each single-phase region is separated by a two-phase coexistence curve which represents the pressure-temperature states where two phases (solid-liquid, liquid-gas, or solid-gas) have equal Gibbs free energy. The triple point, which was calculated independently in Part II, marks the unique pressure-temperature state where all three phases coexist.

Several features of the calculated field-field diagram suggest physically reasonable results for a pure metal. The solid-liquid boundary is vertical, reflecting that the volumes of condensed phases are not pressure dependent which was an assumption made when calculating the P-T phase diagram (note that pressure dependent molar volume was introduced to calculate the V-S phase diagram). The liquid-gas and solid-gas boundaries show nonlinearity, which is consistent with the gas phase's pressure dependence. Comparing the existence of liquid and gas phases, at low pressures, the gas phase is more thermodynamically favorable due to its higher entropy, while higher pressures favor the liquid phase. The triple point occurs at a very low pressure (1.66 Pa) and near the melting temperature of Ni (1814.8 K), which is typical for metals which have high boiling points.

Figure 7 illustrates the field-density (P-S) phase diagram calculated. Here, the two-phase coexistence curves from Figure 6 are transformed into two-phase regions bounded by horizontal tie lies. This is because each point along a phase boundary in P-T space corresponds to a specific entropy value for each phase at the phase boundary. This creates a pair of boundaries that define two-phase areas in P-S space. In P-S space, the tie lines connecting paired phase boundaries are horizontal because each phase still exists as the same pressure (because the thermodynamic state has not changed).

Figure 8 and Figure 9 illustrate the density-density (V-S) phase diagram across two different molar volume and molar entropy ranges to highlight different features of the graph. Figure 8 illustrates the entire V-S phase diagram that maps to the P-T phase diagram plotted while Figure 9 is plotted across a narrower molar volume and molar entropy range near the solid and liquid phases on this phase diagram, which are both small regions in comparison to the solid-gas or solid-liquid two-phase regions on this phase diagram. Like the P-S phase diagram, coexistence curves in P-T space are transformed into two-phase regions. Unlike the P-S phase diagram, these two-phase regions are connected by oblique tie-lines because, although each state exists at a specific pressure, the constant pressure across two different phases results in a different molar volume for each phase.

The oblique tie-lines transform what was a triple point in P-T space and a triple line in P-S space to a triple region in V-S space (triangular region near the center of Figure 8).

The calculated phase diagrams for Ni exhibit the same feature as the example phase diagrams published by Chang, Figure 1. Both show the progression of two-phase coexistence lines to two-phase coexistence regions, and a three-phase coexistence point progressing to a three-phase coexistence line and, ultimately, a three-phase coexistence region. The phase boundaries show similar curvatures to Chang's example and the two-phase regions have similar shapes. These similarities suggest the phase diagrams calculated for Ni correctly capture the fundamental thermodynamics of unary phase equilibria, even if quantitative details may require further refinement.

5. Conclusion

This study successfully calculated unary phase diagrams for Ni using specific heat capacity data, thermophysical properties, and fundamental thermodynamic principles. The methodology involved curve-fitting NIST-JANAF specific heat capacity data to the Shomate equation and deriving enthalpy and entropy functions through integration. A critical improvement over Part II was made to the formulation of extrapolated enthalpy and entropy functions of the solid phase to ensure physically realistic behavior from 0 K to 6000 K. These functions were used to formulate the Gibbs free energy expressions of the solid, liquid, and gas phase from 0 K to 6000 K which were then used to calculate a P-T phase diagram. The P-T phase diagram was translated to P-S and V-S phase diagrams using temperature dependent entropy functions and temperature-pressure dependent molar volume functions for each phase. The calculated diagrams exhibit the expected topological progression, with two-phase coexistence curves transforming into regions and the triple point evolving from a point to a line to a triangular area as the representation changes from field-field to field-density to density-density space.

The calculated phase diagrams demonstrate physically reasonable features. Phase boundaries exhibit appropriate curvature patterns, with nearly vertical solid-liquid boundaries and strongly curved gas boundaries. The proper ordering of phases in entropy and volume space (solid < liquid < gas) was maintained, and the triple point occurs at very low pressure near the melting temperature, typical for metals with high boiling points.

References

[1] B. Hallstedt, "The SGTE collection of binary datasets," *Calphad*, vol. 89, p. 102833, Jun. 2025, doi: https://doi.org/10.1016/j.calphad.2025.102833.

[2] A. Bali, "MTEN 6005 Project Assignment #1 – Pure Element Plots," Sep. 2025.

[3] A. Bali, "MTEN 6005 Project Assignment #2 – Calculating the Triple Point of a Pure Element," Oct. 2025.

[4] *Nist.gov*, 2025. https://janaf.nist.gov/tables/Ni-001.html

[5] M. Dayah, "Periodic Table - Ptable," *ptable.com*, Feb. 06, 2022. https://ptable.com/?lang=en#Properties/Series

[6] "Material Expansion Coefficients." Available: https://psec.uchicago.edu/thermal_coefficients/cte_metals_05517-90143.pdf

[7] "Isothermal Compressibility | The Elements Handbook at KnowledgeDoor," *KnowledgeDoor*, 2025. https://www.knowledgedoor.com/2/elements_handbook/isothermal_compressibility.html (accessed Oct. 30, 2025).

[8] "Create Fit Types for Library Models," *Mathworks.com*, 2021. https://www.mathworks.com/help/curvefit/fittype.html

[9] "Fit curve or surface to data - MATLAB fit," *www.mathworks.com*. https://www.mathworks.com/help/curvefit/fit.html

[10] "Find minimum of constrained nonlinear multivariable function - MATLAB fmincon," *www.mathworks.com*. https://www.mathworks.com/help/optim/ug/fmincon.html

[11] Y. Austin Chang and W. Alan Oates, *Materials Thermodynamics*. John Wiley & Sons, 2010.

[12] balianirudh, "GitHub - balianirudh/materials-thermodynamics-project: Fall 2025 MTEN 6005 materials thermodynamics project," *GitHub*, 2025. https://github.com/balianirudh/materials-thermodynamics-project/tree/main (accessed Oct. 30, 2025).

Appendix

The author's MATLAB code for the MTEN 6005 project is publicly available on GitHub [12].